IEICE TRANS. ELECTRON., VOL. E77–C, NO. 8 AUGUST 1994

PAPER Special Section on Superconducting Devices

Analysis of High-T_c Superconducting Microstrip Antenna Using Modified Spectral Domain Moment Method

Nozomu ISHII†, Toru FUKASAWA† *and* Kiyohiko ITOH†, *Members*

SUMMARY In this paper, we analyze high-T_c superconducting (HTS) microstrip antenna (MSA) using modified spectral domain moment method. Although it is assumed that the patch and the ground plane of the MSA are perfect electric conductors (PECs) in the conventional spectral domain method, we modify this method to compute the conduction loss of the HTS-MSA. In our analysis, the effect of the HTS film is introduced by the surface impedance which we can estimate by using the three fluid model and experimental results. This paper presents numerical results about the HTS-MSA, for example, the relations between the thickness of the substrate and the radiation efficiency, the temperature and the resonant frequency, and so forth. And we discuss the effective power range where the performance of the HTS-MSA is superior to that of the Cu-MSA.

key words: *high-T_c superconducting, microstrip antenna, spectral domain moment method, three-fluid model, radiation efficiency, input impedance*

1. Introduction

In dc state, high-T_c superconductor (HTS) is lossless and its electrical resistance is ideally equal to zero. In ac state, there are some losses in HTS and its resistance is not equal to zero but smaller than good conductor's one at low temperature and low frequency. The surface resistance of HTS is much lower by a factor of 10 to 100 than of Cu at the same temperature for the frequency below 10 GHz. This small resistance allows HTS microwave passive devices to improve the efficiency and to reduce the insertion loss.

In the antenna application, many studies of the HTS antennas have been reported in recent years [1]–[6]. The application of HTS to the microstrip antenna (MSA) has been spotlighted because the efficiency is mainly governed by the conductivity of the patch's conductor as well as the tangent loss of the dielectric [1], [4], [6]. When the substrate is thin or has high permittivity, the dissipated power in the conductors and the dielectric is much larger than the radiated power so that the antenna radiation efficiency drastically falls. Using the HTS film instead of good conductor has a possibility of the efficiency greatly rising if circumstances around the antenna are appropriate for bringing out HTS's performance.

Manuscript received January 22, 1994.
Manuscript revised March 15, 1994.

†The authors are with the Faculty of Engineering, Hokkaido University, Sapporo-shi, 060 Japan.

In this paper, we rigorously estimate the radiation efficiency taking account of all loss terms: radiation, conduction, dielectric and surface wave losses, by using the spectral domain moment method [7]–[9] for the MSA with finite conductivity and the three-fluid model [10] for the HTS film, in the limit where magnetic penetration depth is much smaller than film thickness and the wavelength is much larger than the film thickness.

A numerical estimation of the relation between the radiation efficiency and the thickness of the substrate for an HTS-MSA by using the cavity model was presented [1], provided that the total loss is equal to the sum of all loss terms. This assumption is not always exact so that we estimate that relation again and explain the loss mechanism of the HTS-MSA. And we will show that the resonant frequency of the HTS-MSA is different from that of the Cu-MSA because the magnetic energy is stored in HTS [11], [12].

According to experimental results [13], it is impossible to apply the three-fluid model to the HTS-MSA with large current density. That is, the surface resistance grows larger and the merit of HTS is diminished as the current density is beyond a certain value. It is thus predicted that the upper limit to the input power exists to improve the efficiency by using the HTS film. We will simulate the dependence of the power on both the radiation efficiency and the input impedance and show an existence of the limit to the input power.

2. Modified Spectral Domain Moment Method

In our analysis, a quantity $A(x, y, z)$ in the space domain is related to a quantity $\tilde{A}(k_x, k_y, z)$ in the spectral domain via two-dimensional Fourier transform.

$$\tilde{A}(k_x, k_y, z) = \iint_{-\infty}^{+\infty} A(x, y, z) e^{j(k_x x + k_y y)} dx dy \qquad (1)$$

In the spectral domain, the scattered electric field $\tilde{\mathbf{E}}^s$ by the induced surface current distribution $\tilde{\mathbf{J}}$ on the patch of the MSA shown in Fig. 1, is given by [7]

$$\tilde{E}_x^s = \tilde{G}_{xx}\tilde{J}_x + \tilde{G}_{xy}\tilde{J}_y, \qquad (2)$$

$$\tilde{E}_y^s = \tilde{G}_{yx}\tilde{J}_x + \tilde{G}_{yy}\tilde{J}_y, \qquad (3)$$

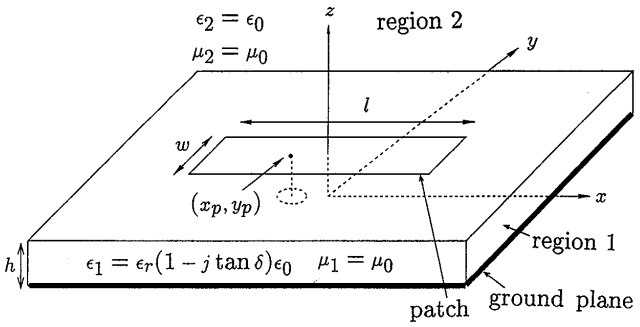

Fig. 1 Structure of microstrip antenna.

at $z = h$, and the incident electric field $\tilde{\mathbf{E}}^i$ by the volume current distribution $\tilde{\mathbf{J}}_i(z) = \hat{z}\tilde{J}_i(z)$ at the probe is given by

$$\tilde{E}_x^i = \int_0^h \tilde{G}_{xz}(z')\tilde{J}_i(z')dz', \tag{4}$$

$$\tilde{E}_y^i = \int_0^h \tilde{G}_{yz}(z')\tilde{J}_i(z')dz', \tag{5}$$

at $z = h$. $\tilde{G}_{xx}, \cdots, \tilde{G}_{yz}$ in Eqs. (2)–(5) are the elements of the dyadic Green's function for the microstrip structure as shown in Fig. 1. These elements can be derived by taking the following boundary conditions into consideration:

1. the impedance boundary conditions $\tilde{E}_x = -Z_{sg}\tilde{H}_y$, $\tilde{E}_y = Z_{sg}\tilde{H}_x$ hold at the ground plane, $z = 0$, where Z_{sg} is the surface impedance for the ground plane.
2. the transverse components of $\tilde{\mathbf{E}}$, $\tilde{\mathbf{H}}$ are continuous at $z = h$.
3. the fields vanish at $z \to \infty$.

The detail of the elements of the Green's function is given in Appendix.

In this paper, we assume that the probe is located at (x_p, y_p) as shown in Fig. 1 and the source current is given by $J_i(x, y, z) = I_p\delta(x - x_p)\delta(y - y_p)$ in the space domain, i.e. $\tilde{J}_i(k_x, k_y, z) = I_p e^{j(k_x x_p + k_y y_p)}$ in the spectral domain, where I_p is a value of the probe current [8], then Eqs. (4) and (5) result in

$$\tilde{E}_x^i = I_p\tilde{G}'_{xz}e^{j(k_x x_p + k_y y_p)}, \tag{6}$$

$$\tilde{E}_y^i = I_p\tilde{G}'_{yz}e^{j(k_x x_p + k_y y_p)}, \tag{7}$$

where

$$\tilde{G}'_{xz} = \int_0^h \tilde{G}_{xz}(z')dz', \tag{8}$$

$$\tilde{G}'_{yz} = \int_0^h \tilde{G}_{yz}(z')dz'. \tag{9}$$

We apply the Galerkin's method to obtain the unknown surface current components $\tilde{J}_x$, $\tilde{J}_y$. First, we expand $\tilde{J}_x$, $\tilde{J}_y$ in the basis functions $\{\tilde{J}_{xm}\}$, $\{\tilde{J}_{yn}\}$ respectively,

$$\tilde{J}_x = \sum_{m=1}^{M} c_m\tilde{J}_{xm}, \tag{10}$$

$$\tilde{J}_y = \sum_{n=1}^{N} d_n\tilde{J}_{yn}, \tag{11}$$

where c_m, d_n are unknown current coefficients which we should determine. At $z = h$, the total electric field $\tilde{\mathbf{E}}^t$ is given by the sum of the incident and the scattered fields,

$$\tilde{\mathbf{E}}^t = \tilde{\mathbf{E}}^i + \tilde{\mathbf{E}}^s. \tag{12}$$

Multiplying the x-component of (12) by $\tilde{J}^*_{xk}$ and the y-component by $\tilde{J}^*_{yl}$, and integrating over k_x and k_y, we can write that

$$\langle\tilde{E}_x^t, \tilde{J}_{xk}\rangle = \langle\tilde{E}_x^i, \tilde{J}_{xk}\rangle + \langle\tilde{E}_x^s, \tilde{J}_{xk}\rangle, \tag{13}$$

$$\langle\tilde{E}_y^t, \tilde{J}_{yl}\rangle = \langle\tilde{E}_y^i, \tilde{J}_{yl}\rangle + \langle\tilde{E}_y^s, \tilde{J}_{yl}\rangle \tag{14}$$

where $k = 1, 2, \ldots, M$, $l = 1, 2, \ldots, N$ and

$$\langle\tilde{E}, \tilde{J}\rangle = \frac{1}{4\pi^2}\iint_{-\infty}^{+\infty}\tilde{E}\,\tilde{J}^* dk_x dk_y \tag{15}$$

corresponds to the reaction of the field $\tilde{E}$ to the source $\tilde{J}$ [14], and the asterisk * indicates complex conjugate. Since

$$\begin{cases} \tilde{E}_x^t = Z_s\tilde{J}_x,\ \tilde{E}_y^t = Z_s\tilde{J}_y & \text{on patch,} \\ \tilde{J}_x = \tilde{J}_y = 0 & \text{otherwise,} \end{cases} \tag{16}$$

at $z = h$, where Z_s is the surface impedance of the patch, Eqs. (13) and (14) can be reduced to

$$-\langle\tilde{E}_x^s - Z_s\tilde{J}_x, \tilde{J}_{xk}\rangle = \langle\tilde{E}_x^i, \tilde{J}_{xk}\rangle, \tag{17}$$

$$-\langle\tilde{E}_y^s - Z_s\tilde{J}_y, \tilde{J}_{yl}\rangle = \langle\tilde{E}_y^i, \tilde{J}_{yl}\rangle, \tag{18}$$

using the Parseval's theorem [7]. Substituting Eqs. (2), (3), (6), (7), (10) and (11) into Eqs. (17) and (18), we can obtain a system of $(M + N)$ linear equations as

$$\sum_{m=1}^{M} c_m Z_{xx}^{(m,k)} + \sum_{n=1}^{N} d_n Z_{xy}^{(n,k)} = V_x^{(k)}, \tag{19}$$

$$\sum_{m=1}^{M} c_m Z_{yx}^{(m,l)} + \sum_{n=1}^{N} d_n Z_{yy}^{(n,l)} = V_y^{(l)}, \tag{20}$$

where $k = 1, 2, \ldots, M$, $l = 1, 2, \ldots, N$ and

$$Z_{xx}^{(m,k)} = -\langle(\tilde{G}_{xx} - Z_s)\tilde{J}_{xm}, \tilde{J}_{xk}\rangle, \tag{21}$$

$$Z_{xy}^{(n,k)} = -\langle\tilde{G}_{xy}\tilde{J}_{yn}, \tilde{J}_{xk}\rangle, \tag{22}$$

$$Z_{yx}^{(m,l)} = -\langle\tilde{G}_{yx}\tilde{J}_{xm}, \tilde{J}_{yl}\rangle, \tag{23}$$

$$Z_{yy}^{(n,l)} = -\langle(\tilde{G}_{yy} - Z_s)\tilde{J}_{yn}, \tilde{J}_{yl}\rangle, \tag{24}$$

$$V_x^{(k)} = I_p\langle\widetilde{G'}_{xz}e^{j(k_x x_p + k_y y_p)}, \tilde{J}_{xk}\rangle, \tag{25}$$

$$V_y^{(l)} = I_p\langle\widetilde{G'}_{yz}e^{j(k_x x_p + k_y y_p)}, \tilde{J}_{yl}\rangle. \tag{26}$$

In matrix form, Eqs. (19) and (20) can be expressed as

$$[Z][I] = [V]. \tag{27}$$

This matrix equation may be solved for the unknown matrix $[I]$ by the inverse, and it can be written as

$$[I] = [Z]^{-1}[V]. \tag{28}$$

Once $[I]$ is found, the input impedance at the probe can be calculated as

$$Z_{in} = [I]^T[V] + jX_L, \tag{29}$$

where ^{T} indicates transpose and X_L is the self-inductance for a coaxial probe as given in Ref. [9]. Using the electric field components $\widetilde{E}_x$, $\widetilde{E}_y$ on the patch and the stationary-phase method [15], the far-field in the spherical coordinates (r, θ, ϕ) is given as

$$E_\theta = \frac{jk_o e^{-jk_o r}}{2\pi r}(\widetilde{E}_x \cos\phi + \widetilde{E}_y \sin\phi), \tag{30}$$

$$E_\phi = \frac{jk_o e^{-jk_o r}}{2\pi r}(-\widetilde{E}_x \sin\phi + \widetilde{E}_y \cos\phi)\cos\theta, \tag{31}$$

where $k_x = k_o \sin\theta\cos\phi$, $k_y = k_o \sin\theta \sin\phi$ and k_o is the wave number in free space. The radiated power is given as

$$P_{rad} = \frac{r^2}{\eta_o}\int_0^{2\pi} d\phi \int_0^{\pi/2} (|E_\theta|^2 + |E_\phi|^2)\sin\theta d\theta, \tag{32}$$

where η_o is the wave impedance in free space. The input power supplied to the antenna is given as

$$P_{in} = \mathrm{Re}\{[I]^T[V]\}. \tag{33}$$

Using the two powers, we can evaluate the radiation efficiency η as the following definition,

$$\eta = \frac{P_{rad}}{P_{in}}. \tag{34}$$

In this paper, the shape of the patch is rectangular so we use the entire basis for the expansion mode as given in Ref. [16]. Numbers of the expansion mode used in Sect. 4 are $M = 1$, $N = 0$.

3. Surface Impedance Estimation for the HTS

The three-fluid model was proposed as the macroscopic model which explains the loss mechanism of HTS and is experimentally valid for the YBCO bulk plate [10]. In this paper, we estimate the surface impedance of YBCO according to this model and published experimental data [10], [13], [17]. An example of the surface impedance of YBCO and Cu is shown in Fig. 2.

If the surface current density on the HTS patch J_s is much larger, we can no longer describe the loss mechanism using the three-fluid model, that is, the surface impedance $Z_s = R_s + jX_s$ becomes a function of J_s as shown in Fig. 3. This experimental result was measured

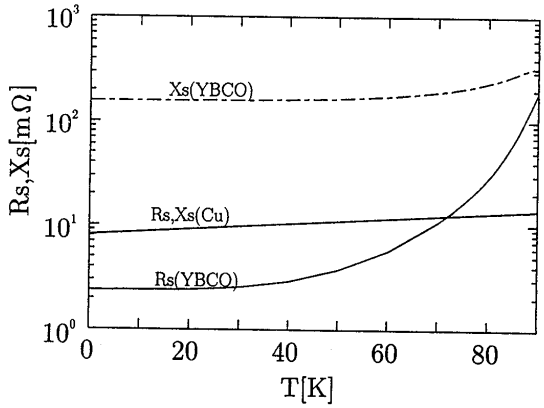

Fig. 2 Temperature vs. surface impedance of YBCO, Cu for $f = 10.4$ GHz, $T_c = 92$ K.

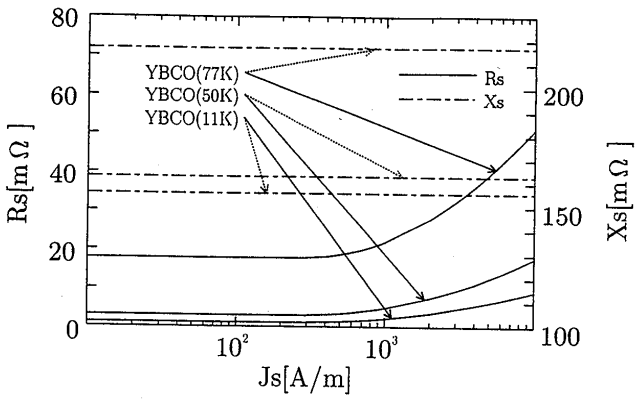

Fig. 3 Surface current density vs. surface impedance of YBCO for $f = 10.4$ GHz.

at 10.4 GHz by Kobayashi et al [13]. From this figure, we can see that although the surface resistance R_s is constant at the temperature below $J_s = 3.0 \times 10^2$ A/m where we can adopt the three-fluid model, R_s becomes larger as J_s increases if J_s is beyond that value. On the contrary, the change of the surface reactance X_s is very small so that we use a constant value of X_s obtained for $J_s \leqq 3.0 \times 10^2$ A/m as the value for $J_s > 3.0 \times 10^2$ A/m.

For $J_s > 3.0 \times 10^2$ A/m, we determine Z_s and J_s as the following procedure. We assume that J_s is flat on the patch. If Z_s is given, we can determine J_s by using the spectral domain moment method as discussed in Sect. 2. We describe this relation as $J_s = f(Z_s)$. On the other hand, if J_s is given, we can determine Z_s by the relation $Z_s = g(J_s)$ shown in Fig. 3. By repeating the two evaluations by turns as a flow chart shown in Fig. 4, we can obtain the surface impedance and the surface current density on the patch. In the following section, we assume that the surface impedance of the ground plane is equal to that of the patch.

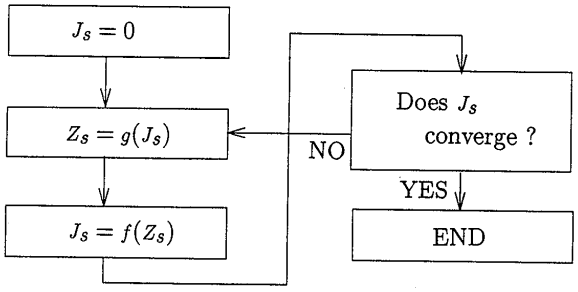

Fig. 4 Algorithm for determining the surface impedance Z_s and the surface current density J_s.

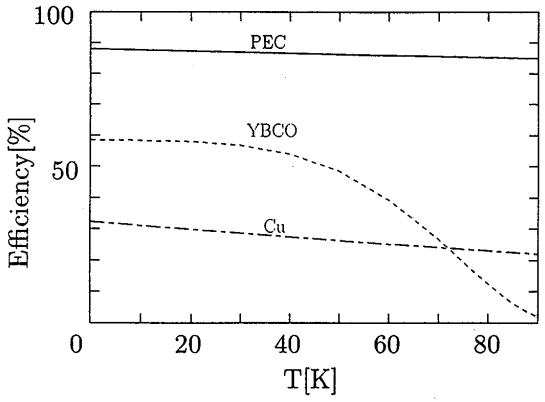

Fig. 5 Temperature vs. efficiency of the PEC-, the YBCO- and the Cu-MSAs for $\epsilon_r \approx 25$, $\tan\delta = 0.5 \sim 3.0 \times 10^{-5}$, $f = 10.4$ GHz. ($l = 3.37$ mm, $w = 0.337$ mm, $h = 0.25$ mm, $x_p = 0.7$ mm, $y_p = 0.0$ mm)

4. Numerical Results

4.1 Temperature versus Efficiency

In Fig. 5, we show the relation between the temperature (T) and the radiation efficiency at 10.4 GHz for three types of MSAs; their patches and ground planes are made of YBCO, Cu and perfect conductor (PEC). The length of the patch is $l = 3.370$ mm, the width of the patch is $w = 0.337$ mm and the thickness of the substrate is $h = 0.25$ mm. We assume that the relative dielectric constant of the substrate is almost $\epsilon_r = 25$ and the loss tangent of the dielectric medium $\tan\delta$ is a function of the temperature as shown in Fig. 2 of Ref. [17].

From Fig. 5, the efficiency of the Cu-MSA decreases gently and almost linearly with T, and that of YBCO-MSA is almost constant for the temperature below 30 K, then begins to fall and eventually goes to less than 10% at 90 K. Thus the radiation efficiency can be improved by using the YBCO film at the temperature not close to the critical temperature $T_c(\approx 90\,\mathrm{K})$, instead of using the Cu film, because the surface resistance of YBCO is much smaller than Cu. For example, we can achieve 1.9 times improvement of the efficiency of the YBCO-MSA at $T = 50$ K respectively.

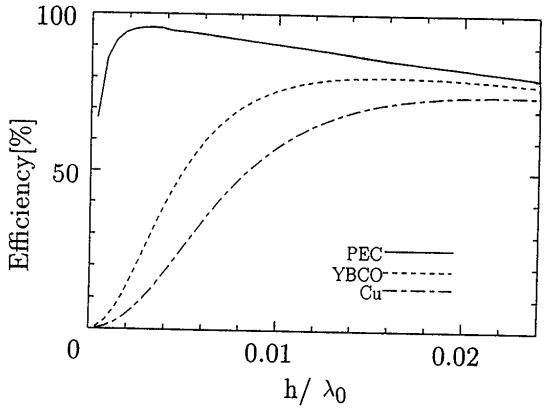

Fig. 6 Substrate thickness h vs. efficiency of the PEC-, the YBCO- and the Cu-MSAs for $\epsilon_r = 5$, $\tan\delta = 1.75 \times 10^{-5}$, $f = 10.4$ GHz, $T = 50$ K. ($l = 7.06$ mm, $w = 0.706$ mm, $h = 0.25$ mm, $x_p = 0.7$ mm, $y_p = 0.0$ mm)

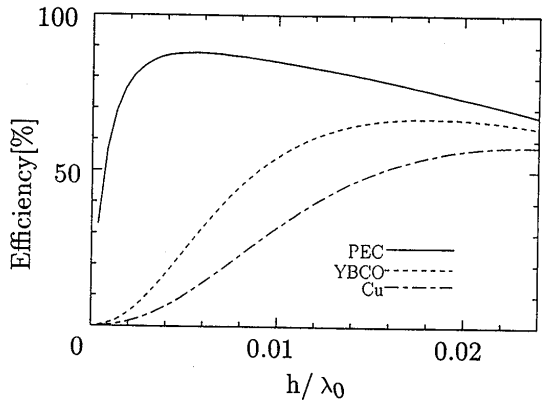

Fig. 7 Substrate thickness h vs. efficiency of the PEC-, the YBCO- and the Cu-MSAs for $\epsilon_r = 25$, $\tan\delta = 1.75 \times 10^{-5}$, $f = 10.4$ GHz, $T = 50$ K. ($l = 3.37$ mm, $w = 0.337$ mm, $h = 0.25$ mm, $x_p = 0.7$ mm, $y_p = 0.0$ mm)

4.2 Thickness of Substrate versus Efficiency

In Figs. 6 and 7, we show the relation between the thickness of the substrate and the radiation efficiency for three types of MSAs: the Cu-, the YBCO-MSAs at 50 K and the PEC-MSA. The patch dimensions l, w are found in order that the resonant frequency of the MSA is about 10.4 GHz under the aspect ratio $l/w = 10$ and $h = 0.25$ mm. The relative dielectric constant of the substrate is $\epsilon_r = 5, 25$ for Figs. 6 and 7 respectively, and the loss tangent is $\tan\delta = 1.75 \times 10^{-5}$.

The efficiency falls off owing to the conduction and the dielectric losses for $h/\lambda_o < 0.005$, where λ_o is the wavelength in free space. In this case, therefore we can achieve a significant increase in efficiency by using the YBCO film with small surface resistance.

As h grows larger, the radiation loss increases so that the radiation efficiency is improved; there is no possibility of the great improvement of the efficiency by using the YBCO film. Furthermore, slight decrease due the surface wave loss in efficiency for $h/\lambda_o > 0.01$ is observed.

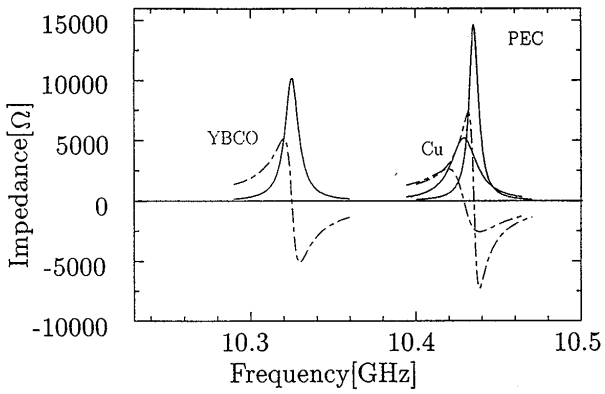

Fig. 8 Input impedance of the PEC-, the YBCO- and the Cu-MSAs for $\epsilon_r = 25$, $\tan\delta = 0.775\times10^{-5}$, $f = 10.4$ GHz, $T = 11$ K. ($l = 3.37$ mm, $w = 0.337$ mm, $h = 0.25$ mm, $x_p = 0.7$ mm, $y_p = 0.0$ mm)

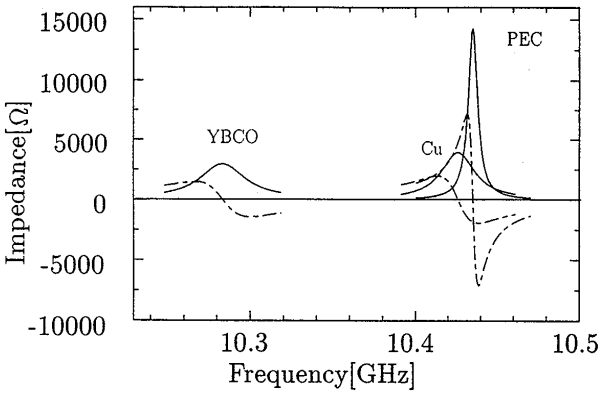

Fig. 9 Input impedance of the PEC-, the YBCO- and the Cu-MSAs for $\epsilon_r = 25$, $\tan\delta = 2.425\times10^{-5}$, $f = 10.4$ GHz, $T = 77$ K. ($l = 3.37$ mm, $w = 0.337$ mm, $h = 0.25$ mm, $x_p = 0.7$ mm, $y_p = 0.0$ mm)

As the dielectric constant of the substrate is lower, the radiated power is larger than the dissipated power so that using the YBCO film may not be effective to improve the efficiency. For example, the efficiency of the YBCO-MSA for $h/\lambda_o = 0.004$ is 2.2 and 2.6 times as large as that of Cu for $\epsilon_r = 5$ and 25 respectively.

4.3 Input Impedance and Resonant Frequency

The input impedance for the PEC-, the Cu- and the YBCO-MSAs at $T = 11, 77$ K is shown in Figs. 8 and 9 respectively. The dimensions of the MSA are the same as the model in Sect. 4.1. These MSAs are driven at $x_p = 0.7$ mm, $y_p = 0.0$ mm by the probe. Because of the conduction loss, the Cu- and the YBCO-MSAs have lower quality factors, wider bandwidths, and lower peaks of the input impedance than the PEC-MSA. However, the quality factor of the YBCO-MSA is rather smaller than the PEC-MSA, although the Cu-MSA has a small quality factor.

Comparing Fig. 8 with Fig. 9, we can see that the resonant frequency of both the YBCO- and the Cu-

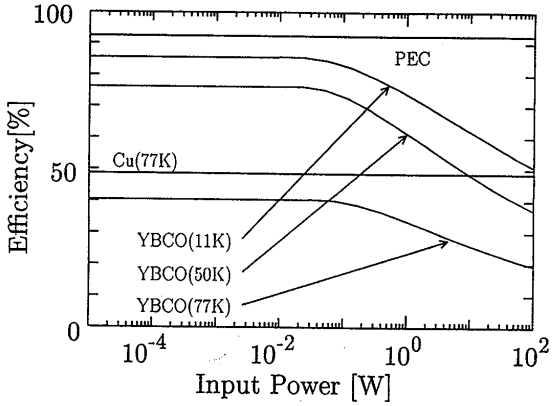

Fig. 10 Input power vs. efficiency of the YBCO-MSA for $\epsilon_r = 5$, $\tan\delta = 0$, $f = 10.4$ GHz, $T = 11, 50, 77$ K. ($l = 7.06$ mm, $w = 0.706$ mm, $h = 0.25$ mm, $x_p = 0.7$ mm, $y_p = 0.0$ mm)

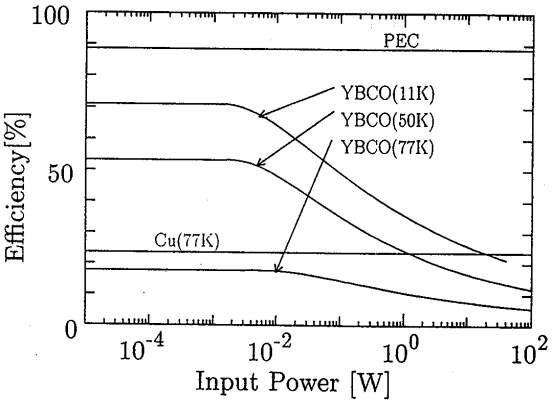

Fig. 11 Input power vs. efficiency of the YBCO-MSA for $\epsilon_r = 25$, $\tan\delta = 0$, $f = 10.4$ GHz, $T = 11, 50, 77$ K. ($l = 3.37$ mm, $w = 0.337$ mm, $h = 0.25$ mm, $x_p = 0.7$ mm, $y_p = 0.0$ mm)

MSAs becomes lower as the temperature increases from 11 K to 77 K. The resonant frequency of the YBCO- and the Cu-MSAs at 77 K is 0.39%, 0.05% lower than that at 11 K. The difference of the shifts is because the dependence of the temperature on the surface reactance X_s of YBCO is much larger than Cu as shown in Fig. 2. In other words, the magnetic energy stored in YBCO is larger than Cu so that a large shift of the resonant frequency is observed in the YBCO-MSA. This is because the kinetic energy stored in the supercurrent which is proportional to the magnetic penetration depth, disturbs the reactive energy balance in the vicinity of YBCO, so that the magnetic energy dominates there.

4.4 Input Power versus Radiation Efficiency

Figures 10 and 11 indicate the radiation efficiency of the YBCO-MSA at 10.4 GHz as a function of the input power P_{in} at $T = 11, 50, 77$ K. The dimensions of the patch l, w are determined in order that the resonant frequency of the MSA with the aspect ratio $l/w = 10$ and $h = 0.25$ mm is about 10.4 GHz. We assume that the dielectric constant of the substrate is $\epsilon_r = 5, 25$ for

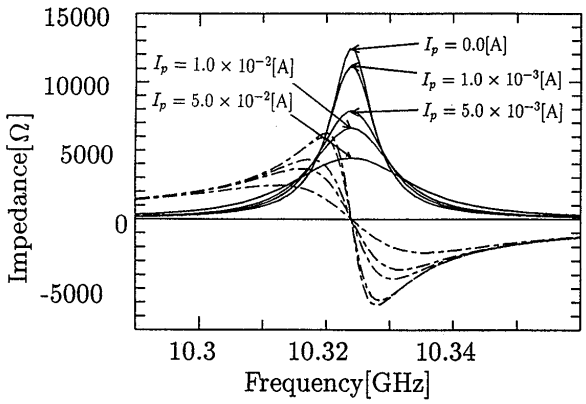

Fig. 12 Probe current I_p vs. input impedance of the YBCO-MSA for $\epsilon_r = 25$, $\tan\delta = 0$, $T = 11$ K. ($l = 3.37$ mm, $w = 0.337$ mm, $h = 0.25$ mm, $x_p = 0.7$ mm, $y_p = 0.0$ mm)

Figs. 10 and 11 respectively.

In the YBCO-MSA, as the input power increases, the surface resistance and the surface current density on the patch are larger so that the radiation efficiency falls down. The efficiency begins to drop at $P_{in} = 3 \times 10^{-2}$, 3×10^{-3} Watts for $\epsilon_r = 5$, 25 respectively. The YBCO-MSA is thus effective for less than a certain power. Furthermore, the permitted limit to the input power is smaller as the dielectric constant ϵ_r is larger. This may be one of factors of preventing the YBCO-MSA from being miniaturized with high ϵ_r substrate.

4.5 Probe Current versus Input Impedance

The relation between the input impedance and the input power at 11 K for the YBCO-MSA with the same dimensions as Sect. 4.4 but $\epsilon_r = 25$ and $\tan\delta = 0$, is shown in Fig. 12. This MSA is driven at $x_p = 0.7$ mm, $y_p = 0.0$ mm by the probe with $I_p = 0.0, 1.0 \times 10^{-3}$, 5.0×10^{-3}, 1.0×10^{-2} and 5.0×10^{-2} A. From this figure, we can see that the quality factor is lower and the peak of the input impedance is smaller but a shift of the resonant frequency is not observed, as the probe current I_p is larger. The latter reason is that the surface reactance is constant for the change of the input power as shown in Fig. 3.

5. Conclusion

We analyze the YBCO-MSA by using the modified spectral domain moment method which can treat of the conduction loss on the patch and the ground plane and the three-fluid model based on the experimental results. From our analysis, we obtain the following results.

- The efficiency of the YBCO-MSA is a few times as large as the Cu-MSA. And using the YBCO film is effective for the microstrip structure with high permittivity and thin substrate which is hard to radiate.
- The peak of the input impedance and the quality factor for the YBCO-MSA are much larger than those for the MSA of good conductor and are slightly smaller than the PEC-MSA. And the resonant frequency of the YBCO-MSA shifts to the lower frequency as the temperature increases owing to the magnetic stored energy in the YBCO film.
- The radiation efficiency decreases as the input power increases, so the application of YBCO to the MSA is effective for less than a certain input power.

References

[1] William, J.T. and Long, S.A., "High Temperature Superconductors and Their Application in Passive Antenna Systems," *IEEE Antennas & Propagat. Magazine*, vol.32, no.4, pp.7–18, Aug. 1990.

[2] Yamaguchi, R., Sawaya, K., Adachi, S. and Ohshima, S., "A Consideration on the Application of High-Temperature Thick-Film Superconductor to Microstrip Array Antenna," *IEICE Technical Report*, A·P90-45, Sep. 1992.

[3] Dinger, R.J., Bowling, D.R. and Martin, A.M., "A Survey of Possible Passive Antenna Applications of High-Temperature Superconductors," *IEEE Trans. Microwave Theory & Tech.*, vol.39, no.9, pp.1498–1507, Sep. 1991.

[4] Chaloupka, H., Klein, N., Peiniger, M., Piel, H., Pischke, A. and Splitt, G., "Miniaturized High-Temperature Superconductor Microstrip Patch Antenna," *IEEE Trans. Microwave Theory & Tech.*, vol.39, no.9, pp.1513–1521, Sep. 1991.

[5] Itoh, K., Ishii, O., Koshimoto, Y. and Cho, K., "High-Temperature Superconducting Small Helical Antenna," *IEICE Trans. Electron.*, vol.E75-C, no.2, pp.246–251, Feb. 1992.

[6] Richard, M.A., Bhasin, K.B. and Claspy, P.C., "Superconducting Microstrip Antennas: An Experiment Comparison of Two Feeding Methods," *IEEE Trans. Antenna & Propagat.*, vol.41, no.7, pp.967–974, Jul. 1993.

[7] Itoh, T. and Menzel, W., "A Full-Wave Analysis Method for Open Microstrip Structures," *IEEE Trans. Antennas & Propagat.*, vol.AP-29, no.1, pp.63–68, Jan. 1981.

[8] Pozar, D.M., "Input Impedance and Mutual Coupling of Rectangular Microstrip Antennas," *IEEE Trans. Antenna & Propagat.*, vol.AP-30, no.6, pp.1191–1196, Nov. 1982.

[9] Deshpande, M.D. and Bailey, M.C., "Input Impedance of Microstrip Antennas," *IEEE Trans. Antenna & Propagat.*, vol.AP-30, no.4, pp.645–650, Jul. 1982.

[10] Kobayashi, Y. and Imai, T., "Phenomenological Description of Conduction Mechanism of High-T_c Superconductors by Three-Fluid Model," *IEICE Trans.*, vol.E74, no.7, pp.1986–1992, Jul. 1991.

[11] Mei, K.K. and Liang, G., "Electromagnetics of Superconductors," *IEEE Trans. Microwave Theory & Tech.*, vol.39, no.9, pp.1545–1552, Sep. 1991.

[12] Iigusa, K., "Analysis of a Resonant Frequency of a Superconducting Circular Microstrip Antenna," *IEICE Trans.*, vol.J74-B-II, no.12, pp.728–730, Dec. 1991.

[13] Kobayashi, Y., Imai, T. and Kayano, H., "Microwave Measurement of Temperature and Current Dependences of Surface Impedance for High-T_c Superconductors," *IEEE Trans. Microwave Theory & Tech.*, pp.1530–1538, Sep. 1991.

[14] Harrington, R.F., *Time-Harmonic Electromagnetic Fields*, p.118, McGraw-Hill, New York, 1961.
[15] Collin, R.E., *Antennas and Radiowave Propagation*, p.168, McGraw-Hill, New York, 1985.
[16] Pozar, D.M. and Voda, S.M., "A Rigorous Analysis of a Microstripline Fed Patch Antenna," *IEEE Trans. Antenna & Propagat.*, vol.AP-35, no.12, pp.1343–1350, Dec. 1987.
[17] Kogami, Y., Kobayashi, Y., Konaka T. and Sato, M., "Low-Loss Bandpass Filter Using Dielectric Rod Resonators Oriented Axially in a High-T_c Superconductor Cylinder," *1991 IEEE MTT-S International Symposium Digest*, RR-6, pp.1345–1348, 1991.

Appendix: Detail of the Elements of the Green's Function

In the appendix, we give concrete expressions for the elements of the Green's function in the spectral domain, which can explain the relation between the electric field at $z = h$ and the electric current density for the microstrip structure as shown in Fig. 1. In the following, the subscripts '1' and '2' (generally denoted by 'i' later) indicate the dielectric and the air regions, respectively.

$$\widetilde{G}_{xx} = -\frac{k_x^2\widetilde{G}_e + k_y^2\widetilde{G}_h}{k_x^2 + k_y^2}, \tag{A·1}$$

$$\widetilde{G}_{xy} = \widetilde{G}_{yx} = -\frac{k_x k_y(\widetilde{G}_e - \widetilde{G}_h)}{k_x^2 + k_y^2}, \tag{A·2}$$

$$\widetilde{G}_{yy} = -\frac{k_y^2\widetilde{G}_e + k_x^2\widetilde{G}_h}{k_x^2 + k_y^2}, \tag{A·3}$$

$$\widetilde{G}_{xz} = -\frac{\omega\mu_1 k_{z2} k_x}{k_1^2 T_m} f_m(z'), \tag{A·4}$$

$$\widetilde{G}_{yz} = -\frac{\omega\mu_1 k_{z2} k_y}{k_1^2 T_m} f_m(z'), \tag{A·5}$$

$$\widetilde{G}_e = \frac{j\omega\mu_1 k_{z1} k_{z2}}{k_1^2 T_m} g_m(h), \tag{A·6}$$

$$\widetilde{G}_h = \frac{j\omega\mu_1}{T_e} g_e(h), \tag{A·7}$$

$$T_m = k_{z2} f_m(h) + j\frac{\epsilon_2}{\epsilon_1} k_{z1} g_m(h), \tag{A·8}$$

$$T_e = k_{z1} f_e(h) + j\frac{\mu_1}{\mu_2} k_{z2} g_e(h), \tag{A·9}$$

$$f_m(z) = \cos k_{z1} z - \frac{j\omega\epsilon_1}{k_{z1}} Z_{sg} \sin k_{z1} z, \tag{A·10}$$

$$g_m(z) = \sin k_{z1} z + \frac{j\omega\epsilon_1}{k_{z1}} Z_{sg} \cos k_{z1} z, \tag{A·11}$$

$$f_e(z) = \cos k_{z1} z + \frac{k_{z1}}{j\omega\mu_1} Z_{sg} \sin k_{z1} z, \tag{A·12}$$

$$g_e(z) = \sin k_{z1} z - \frac{k_{z1}}{j\omega\mu_1} Z_{sg} \cos k_{z1} z, \tag{A·13}$$

where $z'\,(0 \leqq z' \leqq h)$ is the z-coordinate of the source, $k_i = \omega\sqrt{\mu_i\epsilon_i}$, $k_{zi} = \sqrt{k_i^2 + k_x^2 - k_y^2}$, μ_i and ϵ_i are permeability and permittivity in each region i, respectively. In this paper, we set $\mu_1 = \mu_2 = \mu_o$ and $\epsilon_1 = \epsilon_r\epsilon_o(1 - j\tan\delta)$, $\epsilon_2 = \epsilon_o$, where μ_o and ϵ_o are permeability and permittivity in free space, respectively.

Nozomu Ishii was born in Sapporo, Japan, on October 8, 1966. He received the B.S. and M.S. degrees from Hokkaido University, Sapporo, Japan, in 1989, 1991, respectively. In 1991, he joined the faculty of Engineering at Hokkaido University, where he is currently a Research Associate of Electronic Engineering. His current research interests are in the area of numerical analysis of small antenna. He is a member of the IEEE.

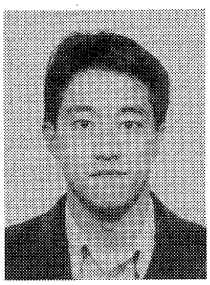

Toru Fukasawa was born in Tokyo, Japan, on December 24, 1969. He received the B.S. and M.S. degrees from Hokkaido University, Sapporo, Japan, in 1992, 1994, respectively. He is presently in Mitsubishi Electric Corporation. When he was in Hokkaido University, his research topics were superconducting small antennas and their numerical analysis.

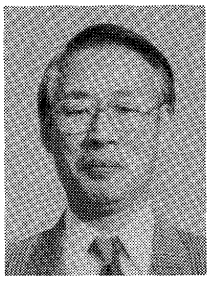

Kiyohiko Itoh was born in Sapporo, Japan, on May 15, 1939. He received the B.S.E.E., M.S., and Ph.D. degrees from Hokkaido University, Sapporo, Japan, in 1963, 1965, and 1973, respectively. Since 1965, he has been on the faculty of Engineering at Hokkaido University, where he is currently a Professor of Electronic Engineering. During 1970–1971, he was with the Department of Electrical and Computer Engineering, Syracuse University, Syracuse, NY, as a Research Associate, on leave from Hokkaido University. His special interests are in electromagnetic radiation, wave optics, mobile communications, and solar power satellites. He is a member of the IEEE and the Institute of Television Engineering of Japan.